Utilisation of Artificial Intelligence in Medical Image Analysis for COVID-19 Patients Detection

Mohammed Baz[1†], Hatem Zaini[1], Hala Abu Zaid[2] and Matokah Abu Al-Naja[3]
[1]Department of Computer Engineering, College of Computer and Information Technology, Taif University, P.O. Box. 11099, Taif [2]1994, Saudi Arabia
[2]Department of Electrical Engineering, Faculty of Engineering, Menoufia University, Shebin El-kom 32511, Egypt
[3]Department of Chemistry, Faculty of Applied Science, Umm Al-Qura University, Makkah, Saudi Arabia

Abstract
Coronavirus (COVID-19) disease constitutes one of the devastating pandemics plaguing humanity throughout the centuries; within about a year since its appearing, the cumulative confirmed cases hit 93 million, whereas the death toll exceeds 2 million. Although several vaccines became available for public worldwide, the speed with which Coronavirus is spread and its different mutant strains hinder stopping its outbreak. This, in turn, prompting the desperate need for devising fast, cheap and accurate tools via which the disease can be diagnosed in its early stage. Reverse Transcription Polymerase Chain Reaction (RTPCR) test is the mainstay tool used to detect the COVID19 symptoms. However, due to the high false-negative rate of this test, physicians employ chest radiographs as an adjunct or alternative tool. Despite the wide-availability, low-cost, and timely radiographs screening results, relying on radiologists to interpret them manually stands against using radiographs as a diagnostic tool. Motivated by the need to speed up the radiographic diagnosis of COVID19 and improves its reliability, this paper proposes a novel deep-learning-based framework dubbed Parallel Deep Neural Networks for Covid-19 Diagnosis (PDNCD). PDNCD integrates the competency of convolution neural networks (CNNs) in treating medical images and the prowess of Recurrent Neural Networks (RNNs) in recognising clinicopathological characteristics to process radiographs and contextual resources simultaneously. By this integration, PDNCD can make perfect classifications even for those cases in which the infection signs in radiographs are unclear due to being the disease in early-stage, confounded by other markers or overlapped by other diseases. Extensive assessments of PDNCD carried out using several datasets demonstrate average diagnostic accuracy of 99.9 accuracies, 0.99 F1-score and near-unity area under the receiver operating characteristic curve.

Keywords:
Covid-19, Artificial intelligence, CNN, RNN

1. Introduction

At the end of 2019, the Coronavirus (COVID-19) caused by the severe acute respiratory syndrome coronavirus 2 (SARS-CoV-2) surprised the world with its rapid spread and catastrophic impact. Within about a year since the appearance of the first case, the number of confirmed cases reaches 93 million, whereas the death toll exceeds 2 million [1]. This pandemic unified the scientists and researchers from all disciplines to curb the spread from all aspects. During the last few months, several institutions and pharmaceutical corporations claimed that safe and effective vaccines became available for the public [2]. However, the hope that the pandemic could be finally defeated has been jeopardised by the appearance of new mutant strains which are more transmissible [3] which might back the pandemic's fighting to square one; indeed, some nations face the second waves and reinforced curfew and lockdown[4]. This promotes the desperate needs for fast, cheap, and accurate tools to diagnose the disease in its early stage.

The key challenge facing rapid diagnoses of COVID-19 is the vast and diverse symptoms presented on patients [5,6] whereas the majority of patients suffer from minor symptoms, (e.g., fever, cough, or tiredness) others might have more severe signs (e.g., loss of movement or shortness of breath) or even no symptoms at all. Hence most of the diagnoses techniques of COVID-19 concentrate on checking whether or not the antigens of this virus are presented in the respiratory of the suspected cases[5-7]. Reverse Transcriptase Polymerase Chain Reaction (RT-PCR) is the standard test in diagnosing of COVID-19 worldwide due to its ability to identify antigens of COVID-19 [7-9]. RT-PCR requires to collect samples from nose or throat and then treats them chemically to isolate and then identify all known viral genetic variations of the disease. Besides, the long time required by the RT-PCR test to produce the results and the limited availability of its kits in some states; it also suffers from a high false-negative ratio (i.e., the situations in which the tests show that the suspected cases are healthy whereas they are infected). Specifically, several research groups estimate this rate as high as 61% [10,11] while other references show that the maximum accuracy of RT-PCR is about 0.8 and can only be obtained on or after the 8th day of symptom onset [10-12].

With the aim to overcome the critical limitations found in the RT-PCP test, chest radiographs are used as an adjunct or alternative diagnostic tool [13,14]. The invaluable information encoded in these images allows the physicians to monitor disease progression rather than determine the infectious status at a single time point as the case in RT-PCR. This makes them suitable for diagnosing

Manuscript received January 5, 2026
Manuscript revised January 20, 2026
https://doi.org/10.22937/IJCSNS.2026.26.1.11

of disease as well as an assessment of its severity [13-17]. Some medical studies show that chest images of COVID-19 patients share some common signs, such as lesions with ground-glass opacities (GGO), lung consolidation, bilateral patchy shadowing, pulmonary fibrosis, multiple lesions and crazy-paving pattern[18,19]. Interestingly, other works were able to infer the severity-degree of the disease from the medical images. For instance, [14-15] shows that during the early stage, the peripheral zone of lungs has multiple small patchy shadows and interstitial changes; while during the progression of diseases multiple Ground-Glass Opacities (GGO) and infiltration start to appear in both lungs and pulmonary consolidation is considered as a sign for a severe case.

One of the key challenges that stand against adopting radiographs as a diagnostic test is the need to examine each image by a radiologist to decide whether the case is infected or not. Estimations for the time and accuracy of the manual examination as introduced in [20] show that a cardiothoracic fellowship-trained radiologist takes around a minute on the average to examine an X-ray image and that the average diagnostic accuracy is about 78%. This is not negligible time, especially when considering that 30 Million tests weekly are required across the states to support the mitigation plan, and other14 Million tests daily are needed as preventive measurements [6,21].

Inspired by the ability of deep learning to automate the diagnosis of several diseases from their medical images e.g., arrhythmia, pneumonia, and fundus image segmentation [22,23]. Numerous models were developed to detect COVID-19 cases, e.g. [24-32]. Most of these models employ the Convolution Neuron Networks (CNN) architecture to extract the common visual hallmarks appearing on the radiograph of patients during the training phase, thereafter the model utilises its gained knowledge to judge new unseen cases. Although these models exhibit high diagnostic reliability; one of the common sources of their performance leakage is inattention of the contextual resources. Annotation, epidemiological history, ages, the clinical manifestation of patients or underlying comorbidities are some attributes that need to be considered when interpreting the radiographs. Several medical studies confirm that the images of patients with different attributes might have different radiographs' signs; for instance [33] shows that the image of COVID-19 pediatric patients has lower pulmonary lobes with higher bronchial wall thickening than adult patients. Whereas [34,35] reported that the image features of COVID-19 could not easily be distinguished in the presence of viral pneumonia, Severe acute respiratory syndrome (SARS) and/or Middle East Respiratory Syndrome (MERS) diseases. Furthermore, Other works report that some contextual factors might confound the deep learning algorithms such as acquisition parameters, projection-type or even presence of tubes, catheters [36].

This paper attempts to overcome the aforementioned challenge by introducing a novel deep learning model dubbed Parallel Deep Neural Networks for Covid-19 Diagnosis (PDNCD). The underlying approach of PDNCD is to treat the images and their contextual resources simultaneously by running two deep learning networks in parallel. Firstly, a CNN, which is deep in spatial, is used to deal with images due to its competency in this domain. Secondly, a Recurrent Neural Network (RNN) [37] which is deep in time, is used to process images' contextual resources. Specifically, RNN has been chosen here due to its ability to consider the inputs' temporal dependencies. Hence changes spotted during the disease progression can be memorised in the network and used to make early prognostic for other cases. Another compelling reason for adopting RNNs in modelling contextual resources is being these networks are not confined to fixed-length inputs or outputs; thus, data of variable length can be treated concurrently. PDNCD is a two-stage architecture in which the first stage is used to build up the medical knowledge from processing contextual resources by RNN and visual features by the CNN to steer the focus in the second stage towards those signs that are significant to confide or dispel diagnostic suspicion. This focal is performed via another CNN and RNN layers whose parameters are tuned based on the previous layers' outputs with the aid of attention mechanisms [38]. Interestingly RNN layers built their knowledge from two sources: specific metadata associated with radiographs and more general COVID-19 corpus. Finally, PDNCD employs concatenate and fully connected layers to consolidate the knowledge gained from the two networks to classify the case either as positive or negative.

According to the best of our knowledge, this is the first work considering using the radiographs' contextual resources to improve the detection capabilities of the COVID-19. In particular, the key contribution of this work can be summarised as:

1- Develop a novel class of deep learning architecture in which medical text from both unstructured (corpus) and structural (metadata of radiographs) in conjunction with spatial information (encoded in radiographs) are processed in parallel to enhance detection capabilities of COVID-19. Besides the advantages of this model in rolling out differential diagnoses of this diseases, the proposed model paves the path towards building more sophisticated models that can be evolved over the time to accommodate updates, e.g., different mutant strains or new diagnosis findings.
2- Reduce the time and computing resources required to train the deep learning model by incorporating the attention mechanism in CNN and RNN networks. Specifically, this mechanism achieves this goal by two

means; firstly expedite approaching the most informative partition of the case that is significant to make a clear diagnosis. Secondly, facilitates treating radiographs at their highest possible resolutions by avoiding use of an image preprocessing technique; hence fine details can be captured accurately.

3- Present comprehensive assessments of the proposed model from different perspectives using several radiographs' datasets [24,26,31,38-50] in addition to a manifold of contextual resources including medical case study, scholarly articles, epidemiological models [51-58]. The results of this assessment demonstrate high capabilities of PDNCD in diagnosing COVID-19 from radiographs with 99.9 accuracies, 0.99 F1-score and near-unity area under the receiver operating characteristic curve.

The remaining of this paper is organised as follows in section II related works are explored, section 3 discusses the methods used to develop PDNCD and asses it. In section 4 the dataset used for assessment of the proposed model in conjunction with results and discussion are presented, and finally, section 5 concludes this work.

2. Related works

Since the appearance of COVID-19 scientists and researchers from artificial intelligence discipline have developed plenty of works and models to curb its outbreak. Here we aim to review some of these works with the aim to highlight approaches underpinned them and point out the merits of our model.

COVIDX-Net[24] is amongst the earliest models introduced to provide rapid diagnoses for COVID19 from x-ray images by combining several pre-trained CNN networks with a binary classifier. COVIDX-Net consists of seven models that are: VGG19, DenseNet201, InceptionV3, ResNetV2, InceptionResNetV2, Xception, and MobileNetV2 each of which is trained and tested individually. Evaluation of the model's performance was conducted over small dataset consisting of preprocessed 50 X-Ray cases, half of them suffering from Covid-19 using 80:20 training to the testing ratio. The key findings of this study demonstrate the capability of pre-trained models to extract the discriminative features of COVID-19 even over a smaller dataset. Furthermore, it is also shown that VGG19 and DenseNet201 have the highest accuracy of 90% whereas the lowest achieved accuracy was 50% due to InceptionV3. Stimulated by the need to improve the diagnosis accuracy using small radiographic datasets, some models employ transfer learning to exploit the knowledge gained from examining individual cases in building a more sensitive classifier. The work in [25] proposed a three layers framework dubbed Decompose, Transfer, and Compose (DeTraC). DeTraC employs two widely used pre-trained CNN models: ImageNet and ResNet to extract the local features appearing in each image individually thereafter passed them to the decompose layer. The underlying approach of this layer is to amplify the irregularities of class boundaries by initiating a sub-class for each distinguished features found previously. The transfer layer with the aid of sophisticated gradient descent optimisation method devised by the authors retrains CNN model using these new sub-classes. Finally, the compose layer is used to assemble subclasses into a single binary class stating whether or not the case is infected with COVID-19. DeTraC is evaluated using several datasets comprising 105 COVID-19, 11 Severe acute respiratory syndromes and 80 normal samples and adopting 70:30 training to the testing ratio. This evaluation demonstrates that DeTraC can attend up to 95.12% overall accuracy. COVIDResNet [26] is another example of models aiming to improve the performance of pre-trained CNN architectures by introducing so-called 3-step fine-tune techniques. The underlying concept of this technique is to resize the input radiographs progressively to different sizes and then adjust the learning parameters accordingly. According to the results reported in the original work, COVIDResNet is able to achieve 96.23% overall accuracy by employing ResNet-50 as a base network over unbalanced dataset consists of 45 COVID-19, 1203 normal, 931 bacterial pneumonia and 660 viral pneumonia patients cases.

The work proposed in [27] employs 11 pre-trained CNNs including AlexNet, GoogleNet, DenseNet, Inception, ResNet, VGG, XceptionNet, and InceptionResNet to extract the key features of the X-Ray images, thereafter pass them to a Support Vector Machine (SVM) which is used to generate the suitable class. The overall accuracy of 95.33% was achieved over balanced dataset consists of 127 COVID-19, 127 pneumonia and 127 normal images that employ 60:20:20 training, validation and testing ratio.

Generative Adversarial Networks (GAN) is a contemporary deep learning approach in which a new sample can be generated from the ground truth dataset. A GAN architecture comprises two models: a generator that is trained to generate new samples and discriminator that attempts to classify the sample as either ground truth or fake (produced by the generator network). Both models compete in a zero-sum game in which the generator endeavours to delude the discriminator about the originality of the sample. The key benefit of GAN in the domain of COVID-19 is to generate new samples from a small dataset; hence, the detectability of the model can be improved. The work presented in [28] employs the GAN approach alongside transfer learning and augmentation process to formulate a three-phase diagnosis architecture. In the first phase, both augmentation and GAN are used to generate new samples that are passed to the second phase in which 4 pre-trained models (i.e., AlexNet, GoogLeNet, Squeeznet, and

Resnet18) are used train the model, and finally, the third phase is used to test the model. The dataset used in this work consists of 5863 X-ray images of two classes, 10% of them are used for training and testing the model, whereas the remaining 90% are generated from the GAN. This work reports that Resnet19 has the highest accuracy of 99% compared to GoogLeNet, AlexNet, and Squeezed. The authors of [29] demonstrate GAN's ability to improve the CNN model's accuracy by more than 10% by introducing two networks. Firstly, a simple CNN constructed from several convolutional layers based on VGG16 architecture followed by the max-pooling and fully connected layers; the model is trained using a small dataset of 331 COVId-19 and 601 normal cases and achieve 85% accuracy. The authors then incorporate this CNN with GAN architecture and allow it to generate 403 of COVID and 721 normal X-ray images; the assessment shows that 95% can be achieved due to this modification. Another work presented in [30] employs a GAN with three pre-trained models: Alexnet, Googlenet, and Restnet18 which are trained using two scenarios of 4 and 3 classes of 307 image, including normal pneumonia bacterial, and pneumonia in additional to COVID-19. The results reported in their works exhibit the outperformance of Googlenet compared to other architectures under 70:20;10 train:test: validation policy.

Building diagnostic models from scratch is another technique that has been introduced in many works; COVID-Net [31] was amongst the pioneer models that adopt this approach. COVID-Net exploits the Projection-Expansion-Projection-eXtension (PEPX) structure of conventional CNN to stack up a large number of convolution layers that can capture meticulous details perfectly. Another crucial advantage of PEPX is its long-range connectivity, which facilities treating large datasets without needing massive computing resources. According to the results reported in this work, 93.3% accuracy level can be achieved over unbalanced, and dataset comprises 183 COVID-19 cases out of 13,800 total images. Additionally, these results show that the sensitivity of COVID-Net is higher than VGG-19 and ResNet-50 by 32% and 8% respectively. COVID-CAPS[32] is another bespoke model that exploits capsule networks' capability in recognising perturbations in the spatial relationships of images. In COVID-CAPS each layer comprises several capsules, each of which uses its own neurons to capture the common features that are usually appeared in a specific partition of the image. COVID-CAPS then employs so-called protocol routing to determine whether or not the desired object is presented in the image. The results shown in this work demonstrate the ability of COVID-CAPS to achieve accuracy of 95.7% using a simple model consists of 4 convolutional and 3 capsules layer without using pretraining. Table 1 summarises some of key findings reported by the peer works.

Table 1: Summary of some peer works

Reference	Number of cases		Pre-processing	Structure	Post-processing	Performance metrics
	COVID-19	Other				
[24]	25	25	Rescaling	7pre-trained CNNs VGG19, ResNetV2, DenseNet201, InceptionV3,, InceptionResNetV2,Xception, and MobileNetV2	N/A	Accuracy=90 Precision =83 F1-Score=91
[25]	105	91	DA, Histogram, Feature Extraction using AlexNet, PCA, K-means	2pre-trained CNNs: ImageNet and ResNet	Composition Phase	Accuracy =95.12 Sensitivity =97.91 Specificity =91.87
[26]	45	2794	DA and Rescaling, Normalizing	ResNet-50	N/A	Accuracy =96.23 Sensitivity =100 Precision =100 F1-Score=100
[27]	127	254	N/A	AlexNet, GoogleNet, DenseNet, Inception, ResNet, VGG, XceptionNet, and InceptionResNet	N/A	Accuracy =95.33 Sensitivity =95.33 F1-Score=95.34
[28]	183	800	Data Augmentation	CNN	Explainabiliy-Driven Audit (GSInquire Method)	Accuracy =93.3 Sensitivity =91
[29]	-	-	N/A	Capsule Layer	N/A	Accuracy =95.7 Sensitivity =90 Specificity =95.8
[30]	58.63	5863	N/A	AlexNet, GoogLeNet, Squeeznet, and Resnet18+ GAN	N/A N/A	Accuracy =99 Precision =98.97 F1-Score=98.97

It can be seen from the above discussion that most of the works presented in the open literature rely on CNN networks to spot the COVID-19 infection signs presented in radiographs. In contrast, this work proposes a novel deep learning model in which both image and both unstructured and structured contextual resources are processing simultaneously. The proposed model employs RNN in parallel with CNN and adopts attraction mechanisms to steer focus dynamically towards those portions of datasets that are significant in making differential diagnoses. According to the best of our knowledge, this is the first work that employs these architectures and techniques to fight COVID-19 outbreak.

3. Methods

The key contribution of this work is to introduce a novel class of deep learning architecture in which contextual resources are utilised in conjunction with the radiographs images to improve diagnostic reliability of COVID-19. Subsection 3.1 is devoted to discussing the method used to develop our proposal where the assessment methods are presented in subsection 3.2.

3.1 The proposed model

The proposed model is dubbed Parallel Deep Neural Networks for Covid-19 Diagnosis (PDNCD) and utilises the deep neuron networks[37] due to their competency in representing a multifaceted system with a high level of accuracy. The building block of these networks is the artificial neuron that was devised to mimic the Biological neuron found in the mammals' nervous system. Typically, each neuron comprises an activation function that maps a given input into the corresponding output by adjusting two learnable parameters: weight and bias. Arranging neurons in different layers and cascading them facilitates expressing a dynamic system as a set of parameters projected over predefined spaces which is known as universal approximation theorem [37-59]. PDNCD concentrates two types of neuron networks: Convolution Neuron networks (CNN) and Recurrent Neuron Networks (RNN). CNN is used to treat images dataset due to its ability to recognise the spatial relationships amongst the samples whereas RNN is used in the domain of natural language processing due to its ability to consider the time-evolving of dynamic systems. Figure 1 illustrates the block diagram of PDNCD.

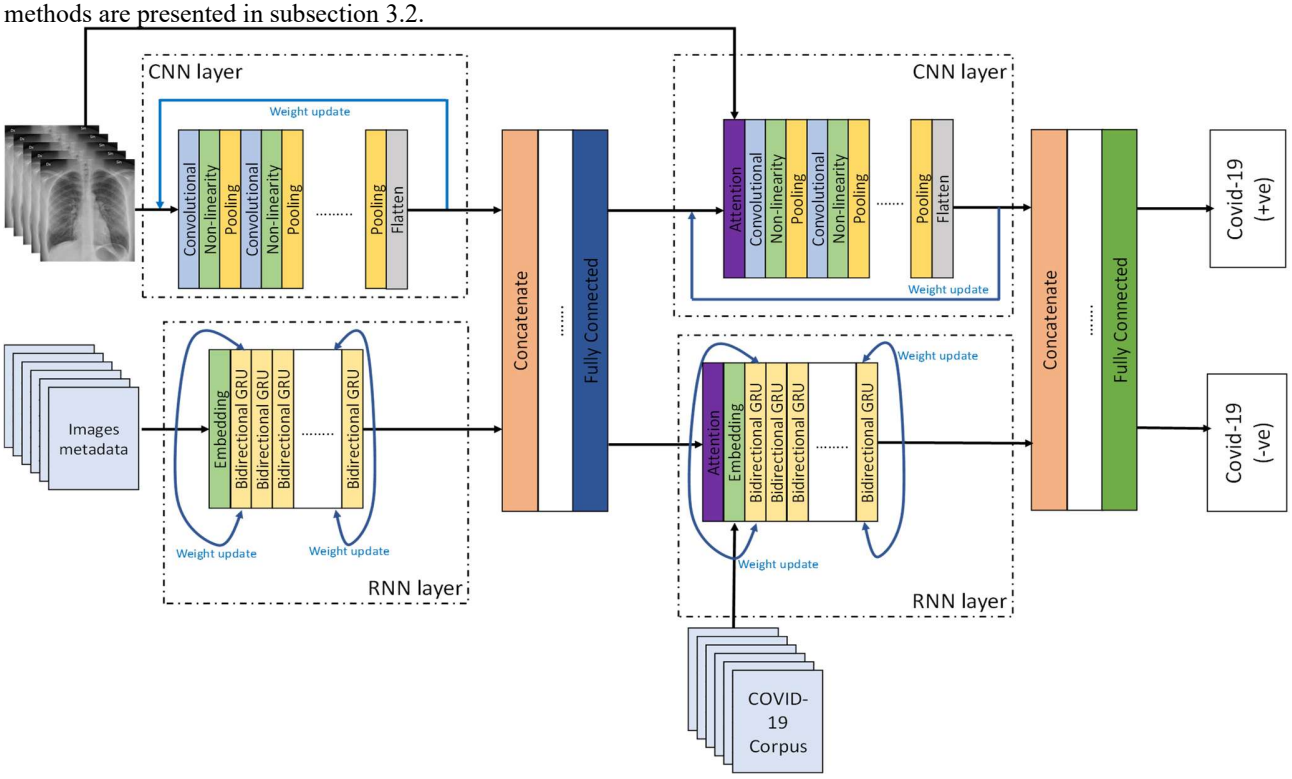

Figure 1 Block diagram of PDNCD

As it can be seen in figure 1 that PDNCD consists of two stages, each of which comprises a CNN and RNN that are running in parallel to process images and textual resources simultaneously. The main aim of the first stage is to construe visual signs spotted in radiographs in relation to descriptions reported in the associated metadata. Thus, the

Manuscript received January 5, 2026
Manuscript revised January 20, 2026
https://doi.org/10.22937/IJCSNS.2026.26.1.11

model can acquire correlations between visual signs and their metadata, which constitutes the medical knowledge required in the subsequent stage.

The CNN of the first stage comprises the following layers: convolutional, non-linearity, pooling, and flatten. The main functionality of the convolutional layer is to extract features exhibited in the images by applying a filter with square Kernal across them. Here twelve kernels with two differnt sizes of 3×3 and 5×5 whose values follow a normal distribution with zero means and unity standard deviation are used for the foremost deeper layer, respectively. The reason behind using larger kernels for deeper layers is that in these layers there is a need to capture closer details by removing the noises at a finer scale. The non-linearity layer is the second important layer that is used to amplify the differences found in the output of the convolutional layer (also known as feature map) by passing them into a non-linear activation function (e.g., hyperbolic tangent tanh or rectified linear unit, ReLU); here we use tanh since it can squash the input into a smaller range$[-1,1]$ whereas compared to a much wider range of ReLU which whose rang is $[0,\infty]$. It is worth noting that, the non-linearity layer does not change the size of the feature maps, rather it prepares them to be ready for further feature extractions by the pooling layer. Fundamentally, pooling layer aims to downsize feature map processed by the non-linearity layer by aggregating a feature represented in several pixels into low dimension pixels. While different operations can be used to achieve such aggregation such as max, min or average pooling layer, this stage of PDNCD employs the maximum pool due to its ability to manifest lighter pixels out of a darker background. Finally, The flatten layer is used to reduce the two-dimensional vectors of spatial features found in the images into a single-dimension to facilitate further processing.

The RNN network of the first stage, as shown in figure 1, consists of two layers: embedding and Bidirectional Gated Recurrent Unit (BGRU). The embedding layer is used to convert the metadata into numerical form so that the neuron networks can process it. This layer employers one hot encoder to express a word into a binary vector of dummy features and then apply the dimension reduction algorithm to minimise the number of these dummy features considering logical interpretation and semantic structure. The BGRU is constructed from two GRUs running side-by-side, the first GRU goes with the forward time directions while the second goes in the reverse direction. By processing the data in both directions, the model can foster its understating for diseases progression without a need to make a chronological order for the data.

The final components of the first stage network are: concatenate and fully connected layers. The concatenate layer is used to connect the outcomes of the upstreaming layers together so that they can be processed jointly by the subsequent layers despite their different lengths. In this stage, the inputs of the concatenate layer are the visual and textual features extracted from the radiographs and their metadata by the CNN and RNN respectively whereas the output of the concatenate layer is a single dimension tensor of their features. Finally, the fully connected layer is a simple network in which each neuron is connected to all neurons in the next layer; hence this topology allows each neuron to consider the information gathered in the previous layer which in turn consolidate the learning and expedite the convergence of the model to the desired outcomes.

The architecture of the second stage of the PDNCD as shown in figure 1 is identical to the first stage except that two attention layers are added in front of CNN and RNN networks and that COVID-19's corpus is used as a dataset for the RNN network instead of the radiographs' metadata. These changes are made to enable PDNCD to exploit the medical knowledge gained in the first stage to focus on those signs that are significant to confide or dispel a diagnostic suspicion. Thus, PDNCD can make perfect classifications even for cases where the infection signs are unclear due to being the disease in early-stage, confounded by other markers or overlapped by other diseases. The attention layers are fully connected networks whose inputs are the outputs of the first stage and whose outputs are the weights of convolutional and embedding layers of the RNN or CNN, respectively. By this arrangement, CNN can extract the more relevant features to the case and RNN can find out the pieces of information that are similar to the case under investigation.

3.2 Assessment methodology

Assessment for the accuracy of the proposed model is carried out here by comparing its outcomes with respect to the ground truth data obtained from the dataset. This assessment uses the following statistical measurements: accuracy, precision, recall, F1-score, Receiver Operating Characteristic (ROC) and Area Under ROC Curve (AUC). The definitions of these metrics are given with the aid of the following terms: True Positive (TP), False Positive (FP), True Negative (TN) and finally False Negative (FN). The TP counts the cases classified by both our proposed model and clinically as patients and TN are the numbers of cases classified by both the model and clinically as healthy. Conversely, FN and (FT) signifies the number of cases that are classified by our model as patients (healthy) whereas clinicians diagnosed them as (healthy) infected.

The accuracy is defined as the ratio of the cases that both models' predictions and physician's diagnoses are agreed with respect to the total cases seen by the model, which can be expressed mathematically as:

$$Accuracy = \frac{TP + TN}{TP + TN + FP + FN} \quad (1)$$

The accuracy metric quantifies the overall effectiveness of a classifier as a function of its ability to make true predictions whether they are positive or negative cases. In the domain of COVID-19, it is highly desired to assess the ability of the model in identifying positive cases so that patients can be isolated to limit further spreading. To address this requirement, precision and recall are used in which the true positive is weighed with respect to other measurements. To be more specific, the precision is a ratio of those cases classified by the model as true in agreement with physician diagnoses to the sum of the positive class predicted by the model either in agreement or disagreement with physicians. Whereas the recall has the same numerator of precision, its denominator comprises the false-negative instead of false-positive as the case in the precision. Expressions for accuracy and precision are given in equations (2) and (3), respectively.

$$\text{precision} = \frac{TP}{TP + FP} \tag{2}$$

$$\text{recall} = \frac{TP}{TP + FN} \tag{3}$$

F1-score is a composed metric that is defined as the harmonic mean of precision and recall, i.e.,

$$\text{F1} - \text{score} = \frac{2TP}{2TP + FP + FN} \tag{4}$$

Equation (4) shows that the maximum value of the F1-score is achieved if both precision and recall are unity, which occurs when both false negative and false positive are zeros. This makes F1-score important when considering unbalanced dataset, i.e., the dataset of which the number of cases of one class is higher than the number of cases belonging to the second class.

Receiver Operating Characteristic (ROC) is a bi-dimensional graph that expresses the recall, which also known as True Positive Rate (TPR) in terms of False Positive Rate (FPR) which are defined.

$$FRP = \frac{FP}{(FP + TN)} \tag{5}$$

ROC's importance emerges from its ability to visualize to what extent the diagnostician differs from random classifier at various threshold settings; hence, two or more models can be compared readily. Finally, the Area Under ROC Curve (AUC) as its name implies, is a measurement for the total area under ROC which ranging from zero to 1.

4. Results and Discussion

This section provides descriptions for the dataset used for the training and testing phases in subsection 4.1 and the results and discussion in subsection 4.2.

4.1 Datasets

With the aim to assess the accuracy of the proposed model from different perspectives, this work utilises several datasets collected from [24,26,31,38-50]. The total number of COVID-19 confirmed, and negative cases used for the training and testing phases are 10,000 and 15,000, respectively. All collected images are combined with randomly ordered and then divided into two mutually exclusive groups along with their metadata: confirmed and COVID-19 negative which are denoted in figure 1 by COVID-19 (+ve) and COVID-19 (-ve) respectively. The former group comprises images of cases, who do not suffer from COVID-19 even if they have other lung diseases; whereas the latter group contains all cases diagnosed as covid-19 patients. The references and repositories used to build contextual resources are 500 case reports from [51-53], 8458 scholarly articles from [54-56] and radiograph annotations from epidemiological models [57-58]. All textual sources are kept in their original formats without a further modification or explanation, whereas the unified medical language system is used as referenceable vocabularies for the embedding layer of RNN. Figure 2 illustrates a sample of case studies reported by [60] showing how the visual signs are changed during the progression of COVID-19.

The datasets are divided randomly into 80% used for training the model and the remaining 20% for the testing purpose; this division was repeated 10 times to form 10-fold cross-validations. Table 2 summarises the key parameters used to conduct the training and testing phases.

Table 2: Summary of key parameters used to train and test

Parameter	Value
Programming Language	Python 3.8 with Tensorflow library.
Environment	Ubuntu machine with Intel(R) Core i9-9900X CPU @ 3.50GHz, 62GB memory and a GeForce RTX 2060 GPU.
optimiser	Adam optimiser
momentum	$\beta_1 = 0.995$ and $\beta_2 = 0.99$
epoch	50
Batch size	32
learning rate	0.0001

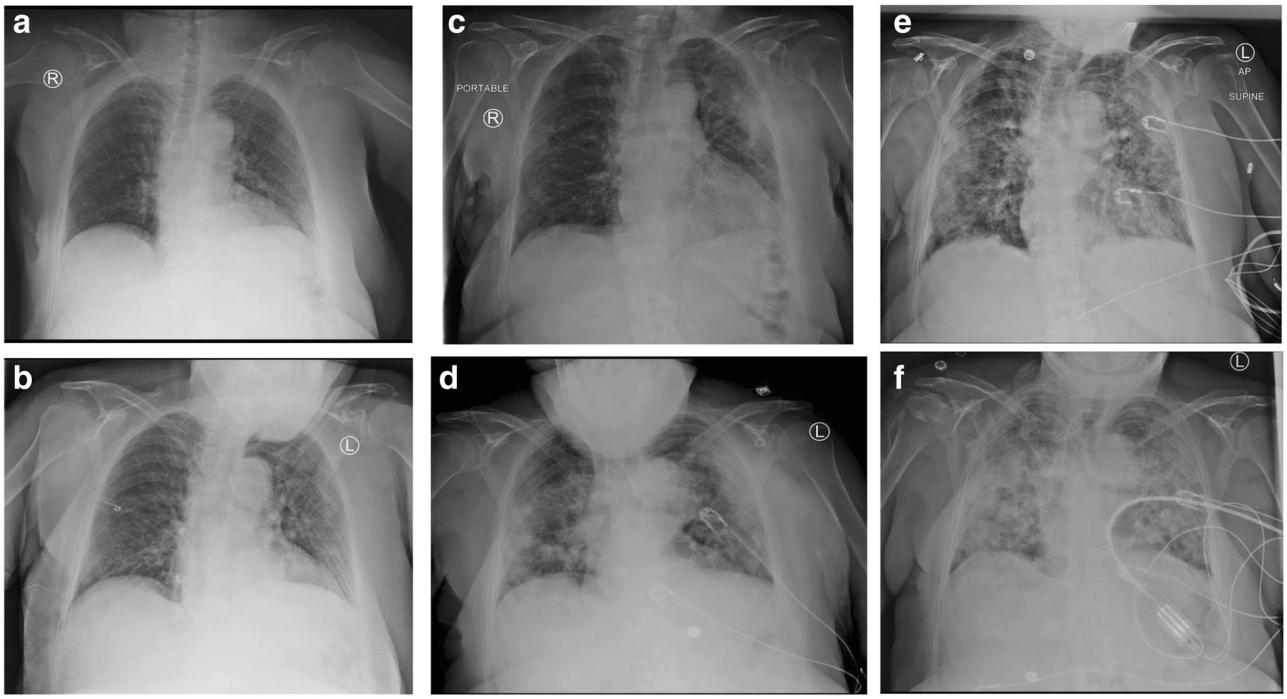

Figure 1 Changes in the visual sings with progression of COVID-19, (a) is taken on the 5th illness day shows peripheral ground-glass opacities in the left lower zone and (b) which is taken 2 days later shows an increase in the diffusely of the ground-glass opacities. Whereas in (c) which is obtained on the 11th day illustrates a further increase and consolidation in the opacities of the left lung with the extension of these opacities to the right lung. On the 14th day of the onset, as shown in (d) shows an enlargement of the reticulations in both lungs with the extension in the right upper zone. the figure (e) which is corresponding to the 17th day depicts intensive bidirectional consolidations and finally (f) shows extensive consolidation in both lungs. Adopted from [60] .

4.2 Results and Discussion

Table 2 summarises readings obtained from assessment the proposed model using the predefined performance metrics. The first column of this table references the source from which the dataset was obtained, whereas the second column presents the aspect ratio which is defined as the percentage of the COVID-19 images to the total images reported in the dataset multiplying by the number of categories of these images. A dataset is considered perfectly balanced if this ratio is one. It is worth noting that the model is trained over the whole datasets from all references; hence, this aspect ratio reflects the percentage used to do the test. The remaining columns give the average readings recorded from all the 10 folds conducting on each dataset.

Table 2. Performance readings of our proposal protocol for different datasets

Reference of dataset	Aspect ratio	Accuracy	Precision	Recall	F_1	AUC
[24]	0.98	$0.98 \pm 1.0 \times 10^{-4}$	$0.93 \pm 3.6 \times 10^{-3}$	$0.93 \pm 3.6 \times 10^{-3}$	$0.96 \pm 4.7 \times 10^{-4}$	$0.99 \pm 3.5 \times 10^{-5}$
[26]	0.95	$0.95 \pm 1.4 \times 10^{-5}$	$0.95 \pm 5.4 \times 10^{-4}$	$0.99 \pm 3.5 \times 10^{-5}$	$0.96 \pm 1.4 \times 10^{-5}$	$0.99 \pm 1.4 \times 10^{-5}$
[31]	2.28	$0.97 \pm 1.5 \times 10^{-6}$	$0.97 \pm 2.3 \times 10^{-4}$	$0.99 \pm 1.4 \times 10^{-5}$	$0.93 \pm 3.6 \times 10^{-3}$	$0.99 \pm 3.5 \times 10^{-5}$
[38]	3.20	$0.93 \pm 1.9 \times 10^{-5}$	$0.99 \pm 3.5 \times 10^{-5}$	$0.95 \pm 5.4 \times 10^{-4}$	$0.95 \pm 5.4 \times 10^{-4}$	$0.98 \pm 3.6 \times 10^{-3}$
[39]	0.98	$0.96 \pm 1.3 \times 10^{-5}$	$0.94 \pm 2.7 \times 10^{-5}$	$0.99 \pm 3.5 \times 10^{-5}$	$0.97 \pm 1.7 \times 10^{-5}$	$0.99 \pm 2.6 \times 10^{-6}$
[40]	0.58	$0.96 \pm 1.4 \times 10^{-5}$	$0.96 \pm 4.7 \times 10^{-4}$	$0.96 \pm 4.7 \times 10^{-4}$	$0.93 \pm 3.6 \times 10^{-3}$	$0.99 \pm 3.5 \times 10^{-5}$
[41]	1.00	$0.97 \pm 1.5 \times 10^{-5}$	$0.94 \pm 4.6 \times 10^{-6}$	$0.93 \pm 3.6 \times 10^{-3}$	$0.99 \pm 1.3 \times 10^{-5}$	$0.99 \pm 5.4 \times 10^{-4}$
[42]	1.20	$0.99 \pm 1.3 \times 10^{-5}$	$0.97 \pm 1.7 \times 10^{-5}$	$0.99 \pm 3.5 \times 10^{-5}$	$0.95 \pm 5.4 \times 10^{-4}$	$0.99 \pm 1.7 \times 10^{-5}$
[43]	0.98	$0.96 \pm 1.2 \times 10^{-5}$	$0.95 \pm 7.1 \times 10^{-6}$	$0.98 \pm 1.4 \times 10^{-5}$	$0.93 \pm 3.6 \times 10^{-3}$	$0.99 \pm 3.5 \times 10^{-5}$
[44]	1.02	$0.95 \pm 1.2 \times 10^{-5}$	$0.99 \pm 2.6 \times 10^{-6}$	$0.95 \pm 5.4 \times 10^{-4}$	$0.97 \pm 1.7 \times 10^{-5}$	$0.99 \pm 2.6 \times 10^{-6}$
[45]	1.90	$0.98 \pm 1.1 \times 10^{-5}$	$0.99 \pm 3.6 \times 10^{-5}$	$0.97 \pm 1.4 \times 10^{-5}$	$0.96 \pm 4.7 \times 10^{-4}$	$0.93 \pm 3.6 \times 10^{-3}$
[46]	4.28	$0.94 \pm 1.0 \times 10^{-5}$	$0.98 \pm 4.6 \times 10^{-6}$	$0.99 \pm 3.5 \times 10^{-5}$	$0.99 \pm 2.6 \times 10^{-6}$	$0.99 \pm 1.3 \times 10^{-5}$
[47]	2.50	$0.98 \pm 1.5 \times 10^{-5}$	$0.99 \pm 8.6 \times 10^{-7}$	$0.97 \pm 1.4 \times 10^{-5}$	$0.97 \pm 1.7 \times 10^{-5}$	$0.99 \pm 5.4 \times 10^{-4}$
[48]	0.12	$0.98 \pm 1.4 \times 10^{-5}$	$0.99 \pm 5.4 \times 10^{-7}$	$0.93 \pm 3.6 \times 10^{-3}$	$0.96 \pm 4.7 \times 10^{-4}$	$0.99 \pm 3.5 \times 10^{-5}$
[49]	0.98	$0.95 \pm 1.2 \times 10^{-5}$	$0.99 \pm 2.6 \times 10^{-6}$	$0.99 \pm 3.5 \times 10^{-5}$	$0.97 \pm 1.7 \times 10^{-5}$	$0.98 \pm 3.6 \times 10^{-3}$
[50]	0.14	$0.99 \pm 3.5 \times 10^{-5}$	$0.95 \pm 5.4 \times 10^{-4}$	$0.93 \pm 3.6 \times 10^{-3}$	$0.99 \pm 1.3 \times 10^{-5}$	$0.99 \pm 5.4 \times 10^{-4}$

Manuscript received January 5, 2026
Manuscript revised January 20, 2026
https://doi.org/10.22937/IJCSNS.2026.26.1.11

A further assessment for our proposal was conducted by comparing the advantage of parallel architecture; two versions of the proposed models were used. Firstly, the PDNCD architecture presented in figure 1 and a modified version of PDNCD in which all RNN networks are removed thus PDNCD was converted to a cascading of CNN networks as the case with other peer works dubbed SDNCD. Comparisons between ROC's of SDNCD and PDNCD for 16 datasets are illustrated in figure 2.

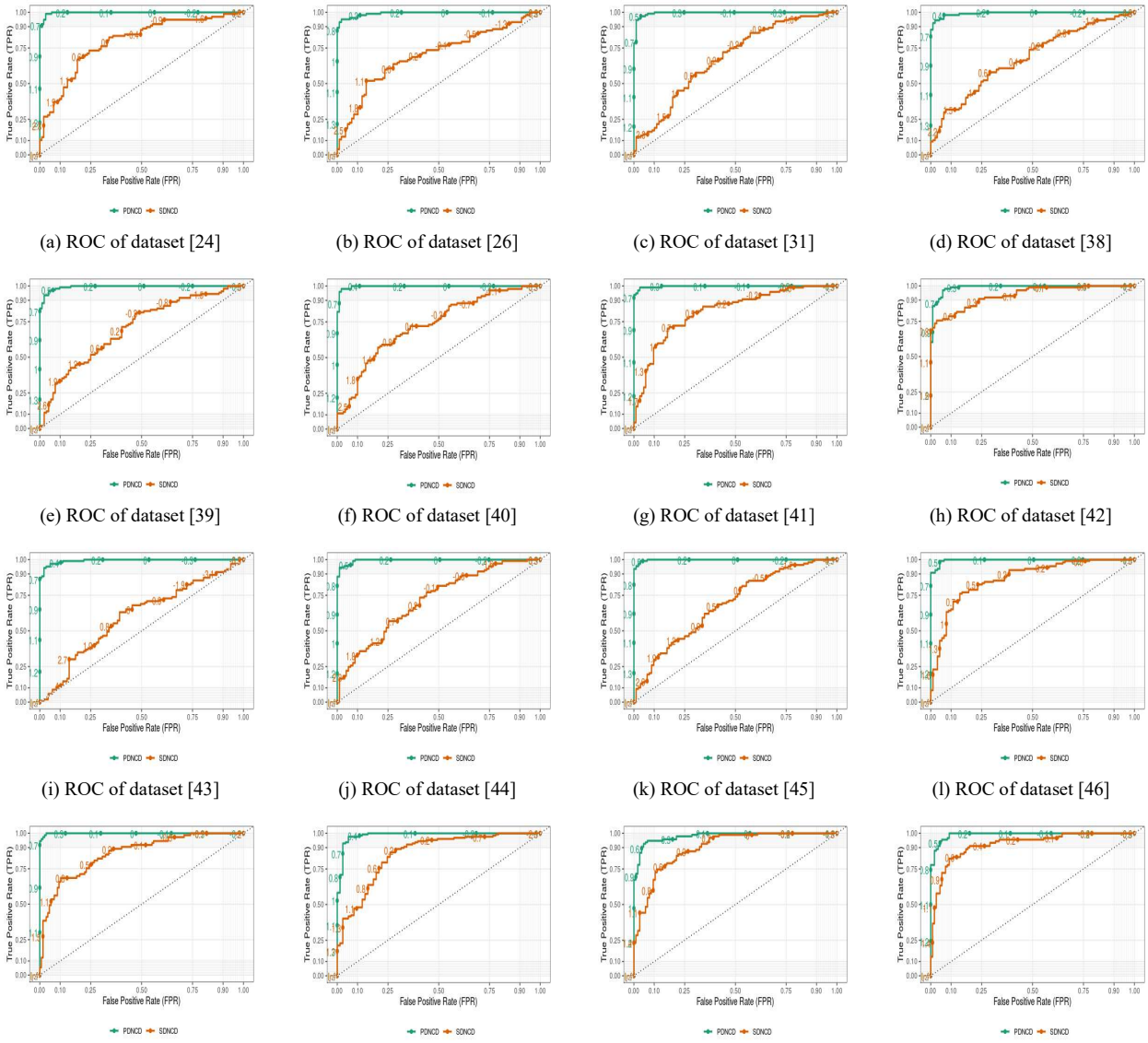

(a) ROC of dataset [24] (b) ROC of dataset [26] (c) ROC of dataset [31] (d) ROC of dataset [38]

(e) ROC of dataset [39] (f) ROC of dataset [40] (g) ROC of dataset [41] (h) ROC of dataset [42]

(i) ROC of dataset [43] (j) ROC of dataset [44] (k) ROC of dataset [45] (l) ROC of dataset [46]

(m) ROC of dataset [47] (n) ROC of dataset [48] (o) ROC of dataset [49] (p) ROC of dataset [50]

Figure 2. ROC of the dataset

As can be seen from the assessment results that the proposed model, PDNCD, exhibits outstanding performance over all datasets. This is attributed mainly to the capability of the parallel architecture to exploit the knowledge gained from both radiographs and contextual resources to improve diagnosis of COVID-19. Another compelling reason for this outperformance is using the attention mechanism in the second stage. This mechanism eliminates a need to employ an image-processing technique which in turn enables PDNCD to extract fine details accurately. It can be seen from table 2 that the aspect ratio has a minor effect of the total performance metrics which is attributed to the ability of PDNCD to make perfect classifications even for cases where the infection signs are unclear due to being the disease in early-stage, confounded by other markers or overlapped by other diseases. Hence,

Manuscript received January 5, 2026
Manuscript revised January 20, 2026
https://doi.org/10.22937/IJCSNS.2026.26.1.11

CNN can extract the more relevant features to the case and RNN can find out the pieces of information that are similar to the case under investigation despite the size of the sample fed into the model. Figure 2 shows that removing the parallel architecture from PDNCD can degrade the performance of the classification significantly. Since inattention of the contextual resources yields a week model that depends on spotting the visual signs that might be overlapped by other markers.

5. Conclusion

This paper proposed a novel deep learning model dubbed Parallel Deep Neural Networks for Covid-19 Diagnosis (PDNCD) whose underlying approach is to treat the images and their contextual resources simultaneously by running two CNN and RNN networks in parallel. PDNCD is a two-stage architecture in which the first stage is used to build up the medical knowledge from processing contextual resources by RNN and visual features by the CNN to steer the focus in the second stage towards those signs that are significant to confide or dispel diagnostic suspicion. This focal is performed via another CNN and RNN layers whose parameters are tuned based on the previous layers' outputs with the aid of attention mechanisms. According to the best of our knowledge, this is the first work considering using the radiographs' contextual resources to improve the detection capabilities of the COVID-19. Comprehensive assessments of the proposed model from different perspectives demonstrate the high capabilities of PDNCD in diagnosing COVID-19.

Acknowledgments

This work was supported by the research project grant number (1-441-61), funded by the Deanship of Scientific Research, Taif University, ministry of reduction, Saudi Arabia..

References

[1] Coronavirus Disease (COVID-19) Dashboard, World Health Organization, January .2021. [Online]. Available: https://covid19.who.int/

[2] Vaccines and immunization: What is vaccination? World Health Organization, January .2021. [Online]. Available: https://bit.ly/38XIo2r

[3] Mutant coronavirus in the United Kingdom sets off alarms, but its importance remains unclear, American Association for the Advancement of Science, January .2021. [Online]. Available: https://bit.ly/3iyMPE7

[4] Christelle Baunez, Mickael Degoulet, Stéphane Luchini, Patrick A. Pintus, Miriam Teschl medRxiv 2020.11.11.20230243; doi: https://doi.org/10.1101/2020.11.11.20230243

[5] Gao Z, Xu Y, Sun C, et al. A Systematic Review of Asymptomatic Infections with COVID-19 [published online ahead of print, 2020 May 15]. J Microbiol Immunol Infect. 2020;10.1016/j.jmii.2020.05.001.doi:10.1016/j.jmii.2020.05.001.

[6] National Academies of Sciences, Engineering, and Medicine. 2020. Rapid Expert Consultation on Critical Issues in Diagnostic Testing for the COVID-19 Pandemic (November 9, 2020). Washington, DC: The National Academies Press. https://doi.org/10.17226/25984.

[7] Verma, N., Patel, D. & Pandya, A. Emerging diagnostic tools for detection of COVID-19 and perspective. Biomed Microdevices 22, 83 (2020). https://doi.org/10.1007/s10544-020-00534-z.

[8] Doak SH, Zaïr ZM. Real-time reverse-transcription polymerase chain reaction: technical considerations for gene expression analysis. Methods Mol Biol. 2012;817:251-70. doi: 10.1007/978-1-61779-421-6_13. PMID: 22147577.

[9] Ghossein R.A., Bhattacharya S., Coit D.G. (2001) Reverse Transcriptase Polymerase Chain Reaction (RT-PCR) Detection of Melanoma-Related Transcripts in the Peripheral Blood and Bone Marrow of Patients with Malignant Melanoma. What Have We Learned?. In: Reinhold U., Tilgen W. (eds) Minimal Residual Disease in Melanoma. Recent Results in Cancer Research, vol 158. Springer, Berlin, Heidelberg. https://doi.org/10.1007/978-3-642-59537-0_7

[10] Bahreini F, Najafi R, Amini R, Khazaei S, Bashirian S. Reducing False Negative PCR Test for COVID-19. Int J MCH AIDS. 2020;9(3):408-410. doi:10.21106/ijma.421

[11] Mallett, S., Allen, A.J., Graziadio, S. et al. At what times during infection is SARS-CoV-2 detectable and no longer detectable using RT-PCR-based tests? A systematic review of individual participant data. BMC Med 18, 346 (2020). https://doi.org/10.1186/s12916-020-01810-8

[12] Wikramaratna Paul S, Paton Robert S, Ghafari Mahan, Lourenço José. Estimating the false-negative test probability of SARS-CoV-2 by RT-PCR. Euro Surveill. 2020;25(50):pii=2000568. https://doi.org/10.2807/1560-7917.ES.2020.25.50.2000568.

[13] National Health Commission & National Administration of Traditional Chinese Medicine. Diagnosis and Treatment Protocol for Novel Coronavirus Pneumonia (Trial Version 7) [J]. Chin Med J,2020,133 (09): 1087-1095. DOI: 10.1097/CM9.0000000000000819.

[14] Yasin, R., Gouda, W. Chest X-ray findings monitoring COVID-19 disease course and severity. Egypt J Radiol Nucl Med 51, 193 (2020). https://doi.org/10.1186/s43055-020-00296-x

[15] Wasilewski PG, Mruk B, Mazur S, Półtorak-Szymczak G, Sklinda K, Walecki J. COVID-19 severity scoring systems in radiological imaging - a review. Pol J Radiol. 2020;85:e361-e368. Published 2020 Jul 17. doi:10.5114/pjr.2020.98009

[16] Cozzi D, Albanesi M, Cavigli E, et al. Chest X-ray in new Coronavirus Disease 2019 (COVID-19) infection: findings and correlation with clinical outcome. Radiol Med. 2020;125(8):730-737. doi:10.1007/s11547-020-01232-9

[17] Wang, J., Zhu, X., Xu, Z. et al. Clinical and CT findings of COVID-19: differences among three age groups. BMC Infect Dis 20, 434 (2020). https://doi.org/10.1186/s12879-020-05154-9

[18] Hefeda, M.M. CT chest findings in patients infected with COVID-19: review of literature. Egypt J Radiol Nucl Med 51, 239 (2020). https://doi.org/10.1186/s43055-020-00355-3

[19] Carotti M, Salaffi F, Sarzi-Puttini P, et al. Chest CT features of coronavirus disease 2019 (COVID-19) pneumonia: key points for radiologists. Radiol Med. 2020;125(7):636-646. doi:10.1007/s11547-020-01237-4
[20] Northwestern University. "AI detects COVID-19 on chest X-rays with accuracy and speed: Algorithm outperformed thoracic radiologists in new study." ScienceDaily. ScienceDaily, 24 November 2020.
[21] Stein, R. 2020. Can the US use its growing supply of rapid tests to stop the virus? National Public Radio, October 1. https://www.npr.org/sections/health-shots/2020/10/01/915793729/can-the-u-s-use-its-growing-supply-of-rapid-tests-to-stop-the-virus (accessed October 24, 2020).
[22] Litjens G, Kooi T, Bejnordi BE, Setio AAA, Ciompi F, Ghafoorian M, van der Laak JAWM, van Ginneken B, Sánchez CI. A survey on deep learning in medical image analysis. Med Image Anal. 2017 Dec;42:60-88. doi: 10.1016/j.media.2017.07.005. Epub 2017 Jul 26. PMID: 28778026.
[23] Shen D, Wu G, Suk HI. Deep Learning in Medical Image Analysis. Annual Review of Biomedical Engineering. 2017 Jun;19:221-248. DOI: 10.1146/annurev-bioeng-071516-044442
[24] Hemdan E. E.-D., Shouman M. A. & Karar M. E. COVIDX-Net: A framework of deep learning classifiers to diagnose COVID-19 in X-ray images. arXiv:2003.11055 (2020).
[25] A. Abbas, M. M. Abdelsamea and M. M. Gaber, "DeTrac: Transfer Learning of Class Decomposed Medical Images in Convolutional Neural Networks," in IEEE Access, vol. 8, pp. 74901-74913, 2020, doi: 10.1109/ACCESS.2020.2989273.
[26] Farooq, M., & Hafeez, A. (2020). COVID-ResNet: A Deep Learning Framework for Screening of COVID19 from Radiographs. ArXiv, abs/2003.14395.
[27] Sethy, P.K.; Behera, S.K.; Ratha, P.K.; Biswas, P. Detection of Coronavirus Disease (COVID-19) Based on Deep Features and Support Vector Machine. Preprints 2020, 2020030300
[28] Khalifa, N.E.; Taha, M.H.; Hassanien, A.E.; Elghamrawy, S. Detection of Coronavirus (COVID-19) Associated Pneumonia based on Generative Adversarial Networks and a Fine-Tuned Deep Transfer Learning Model using Chest X-ray Dataset. arXiv 2020, arXiv:2004.01184
[29] A. Waheed, M. Goyal, D. Gupta, A. Khanna, F. Al-Turjman and P. R. Pinheiro, "CovidGAN: Data Augmentation Using Auxiliary Classifier GAN for Improved Covid-19 Detection," in IEEE Access, vol. 8, pp. 91916-91923, 2020, doi: 10.1109/ACCESS.2020.2994762.
[30] Loey, M.; Smarandache, F.; M. Khalifa, N.E. Within the Lack of Chest COVID-19 X-ray Dataset: A Novel Detection Model Based on GAN and Deep Transfer Learning. Symmetry 2020, 12, 651. https://doi.org/10.3390/sym12040651
[31] Wang, L., Lin, Z.Q. & Wong, A. COVID-Net: a tailored deep convolutional neural network design for detection of COVID-19 cases from chest X-ray images. Sci Rep 10, 19549 (2020). https://doi.org/10.1038/s41598-020-76550-z
[32] Afshar, P.; Heidarian, S.; Naderkhani, F.; Oikonomou, A.; Plataniotis, K. N.; and Mohammadi, A. 2020. Covid-caps: A capsule network-based framework for identification of covid-19 cases from x-ray images. arXiv preprint arXiv:2004.02696.
[33] Chen A, Huang J, Liao Y et al. Differences in Clinical and Imaging Presentation of Pediatric Patients with COVID-19 in Comparison with Adults. Radiol Cardiothorac Imaging 2020;2(2):e200117.
[34] Luo, L., Luo, Z., Jia, Y. et al. CT differential diagnosis of COVID-19 and non-COVID-19 in symptomatic suspects: a practical scoring method. BMC Pulm Med 20, 129 (2020). https://doi.org/10.1186/s12890-020-1170-6
[35] American Roentgen Ray Society. "Novel coronavirus (COVID-19) imaging features overlap with SARS and MERS: COVID-19's imaging features are variable and nonspecific, but the imaging findings reported thus far do show." ScienceDaily. ScienceDaily, 28 February 2020.
[36] Aurelia Bustos, Antonio Pertusa, Jose-Maria Salinas, and Maria de la Iglesia-Vay´a.Padchest: A large chest x-ray image dataset with multi-label annotated reports. arXiv preprint arXiv:1901.07441, 2019.
[37] Ian Goodfellow, Yoshua Bengio, Aaron Courville, Deep Learning, MIT Press, 2018.
[38] German Creamer, Gary Kazantsev, Tomaso Aste, Machine Learning and AI in Finance, Routledge, 2021
[39] Muhammad Chowdhury, Tawsifur Rahman, Amith Khandakar, Rashid Mazhar, Muhammad Kadir, Zaid Mahbub, Khandakar Islam, Muhammad Salman Khan, Atif Iqbal, Nasser Al-Emadi, and Mamun Bin Ibne Reaz. Can AI help in screening viral and COVID-19 pneumonia? IEEE Access, 8:132665–132676, 03 2020.
[40] Joseph Paul Cohen, Paul Morrison, Lan Dao, Karsten Roth, Tim Q Duong, and Marzyeh Ghassemi. COVID-19 Image Data Collection: Prospective Predictions Are the Future. arXiv 2006.11988, 2020.
[41] Tulin Ozturk, Muhammed Talo, Eylul Azra Yildirim, Ulas Baran Baloglu, Ozal Yildirim, and U. Rajendra Acharya. Automated detection of COVID-19 cases using deep neural networks with X-ray images. Computers in Biology and Medicine, 121(April):103792, 2020.
[42] Aurelia Bustos, Antonio Pertusa, Jose-Maria Salinas, and Maria de la Iglesia-Vayá. PadChest: A large chest x-ray image dataset with multi-label annotated reports. Medical Image Analysis, 66:101797, 2020.
[43] G. Inc. Github. Website, May 2020. https://github.com
[44] I. S. . ore. The coronavirus datasets in italy. Website, May 2020. https://lab24.ilsole24ore.com/coronavirus
[45] T. R. Novel corona virus 2019 dataset. Website, May 2020. https://www.kaggle.com/tawsifurrahman/covid19-radiography-database.
[46] Radiopaedia. Images of covid-19 cases. Mendeley Data, May 2020. https://radiopaedia.org.
[47] M. Segmentation. Covid-19 ct segmentation dataset. Website, May 2020. http://medicalsegmentation.com/covid19.
[48] J. Zhao, Y. Zhang, X. He, and P. Xie. Covid-ct-dataset: a ct scan dataset about covid-19. arXiv preprint arXiv:2003.13865, 2020. https://github.com/UCSD-AI4H/COVID-CT.
[49] J. Chen, L. Wu, J. Zhang, L. Zhang, D. Gong, Y. Zhao, S. Hu, Y. Wang, X. Hu, B. Zheng, and K. Zhang, ``Deep learning-based model for detecting 2019 novel coronavirus pneumonia on high-resolution computed tomography: A prospective study," MedRxiv, Mar. 2020, doi: 10.1101/2020.02.25.20021568.

[50] X. Chen, L. Yao, and Y. Zhang, \Residual attention u-net for automated multi-class segmentation of covid-19 chest ct images," arXiv preprint arXiv:2004.05645, 2020.

[51] Covid-19 open research dataset challenge (cord19). https://www.kaggle.com/allen-institute-for-ai/ CORD-19-research-challenge/discussion/139427. Accessed: 2010-09-30.

[52] Boccaletti S, Ditto W, Mindlin G, Atangana A (2020) Modeling and forecasting of epidemic spreading: the case of covid-19 and beyond. Chaos, Solitons, and Fractals

[53] He J, He L, Zhou W, Nie X, He M (2020) Discrimination and social exclusion in the outbreak of covid-19. Int J Environ Res Public Health 17(8):2933.

[54] Wynants L, Van Calster B, Bonten MMJ, Collins GS, Debray TPA, De Vos M, Haller MC, Heinze G, Moons KGM, Riley RD et al (2020) Prediction models for diagnosis and prognosis of covid-19 infection: systematic review and critical appraisal. bmj, 369

[55] Dong E, Du H, Gardner L (2020) An interactive web-based dashboard to track covid-19 in real time. The Lancet infectious diseases.

[56] Kleinberg B, van der Vegt I, Mozes M (2020) Measuring emotions in the covid-19 real world worry dataset. arXiv:2004.04225.

[57] Chen E, Lerman K, Ferrara E (2020) Covid-19:, The first public coronavirus twitter dataset. arXiv:2003.07372 Zarei K, Farahbakhsh R, Crespi N, Tyson G (2020) A first instagram dataset on covid-19. arXiv:2004.12226

[58] Sarker A, Lakamana S, Hogg-Bremer W, Xie A, Al-Garadi MA, Yang Y-C (2020) Self-reported covid-19 symptoms on twitter: An analysis and a research resource. medRxiv

[59] Hornik, K., Stinchcombe, M., and White, H.: Multilayer Feedforward Neural Networks Are Universal Approximators, Neural Networks 2 (1989), pp. 359–366

[60] Rousan, L.A., Elobeid, E., Karrar, M. *et al.* Chest x-ray findings and temporal lung changes in patients with COVID-19 pneumonia. *BMC Pulm Med* **20,** 245 (2020). https://doi.org/10.1186/s12890-020-01286-5.

.